Materials & Design 258 (2025) 114584

Contents lists available at ScienceDirect

Materials & Design

journal homepage: www.elsevier.com/locate/matdes

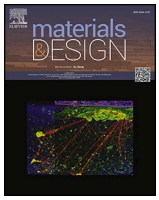

How surface treatment of porous copper samples dictates dry friction and wear

Roxane Lung, Karl Günter Schell, Christian Greiner *

Institute for Applied Materials (IAM), Karlsruhe Institute of Technology (KIT), Karlsruhe 76131, Germany

ARTICLE INFO

Keywords:
Roughness
Polishing
Porosity
Copper
Tribology
Friction
Wear

ABSTRACT

Surface treatments such as electropolishing and chemical–mechanical vibropolishing are widely used to enhance surface quality in medical technology, semiconductor, and aerospace. Copper, commonly used in heat exchangers and electronics, can benefit from improved tribological behavior to increase efficiency, reliability, and lifespan. This study investigates how surface treatments affect tribological performance and evaluates the long-term effectiveness of the more promising treatment. Specimens with varying porosity were either vibropolished or electropolished and tested using a reciprocating ball-on-flat tribometer for 1000 and 5000 cycles. Electropolishing enlarged sintering pores. This led to an increase in S_a from 0.1 to 1.6 μm, higher surface stresses, as well as more deformation; causing deeper wear tracks and pronounced grooves, smeared pores, and finer grains. These friction-induced changes include formation of new grain boundaries, promoting tribo-oxidation, cracking, and delamination. In contrast, vibropolished surfaces show minimal subsurface deformation. These mechanisms correlate with a coefficient of friction of 0.25 after vibropolishing and 0.65 after electropolishing. Long-term performance was assessed by examining whether vibropolished specimens, despite minimal subsurface deformation, behave similarly to electropolished ones. High-porosity vibropolished samples kept friction below 0.3 over 5000 cycles, despite increased tribo-oxidation, while the low-porosity one developed cracks, delamination, maintaining high friction around 0.65.

1. Introduction

In many application fields, the surface of workpieces is processed to achieve a high-quality surface finish. Both electropolishing and chemical–mechanical vibropolishing are widely used for this purpose. During electropolishing, the workpiece is made anodic in a most often high-viscosity concentrated acid solution, which may contain phosphoric acid [1–3]. Due to the applied voltage, a significant portion of the electric charge accumulates at the asperities of the surface roughness, causing the edges to dissolve first [4]. Electropolishing is widely used in industrial applications to achieve very smooth surfaces, due to its simplicity, and because it can be applied to complex structures [1,5,6]. It is employed in various industries, including the food industry, medical technology, such as in stainless steel surgical devices, as well as in the semiconductor industry for optical, electrical and ultra-high vacuum components, and in the pharmaceutical industry. Additionally, it is used to remove preparation-induced deformation layers before examining specimens, such as those analyzed with electron backscatter diffraction. During chemical–mechanical polishing, both a chemical reaction and mechanical material removal occur [7,8]. According to Steigerwald et al. [9], clusters of atoms are first mechanically removed by abrasive particles from the specimen surface and then chemically dissolved. While an insufficient chemical polishing may cause the sample surface to be scratched again, a more intense chemical reaction can lead to both increased surface roughness and difficulty in achieving planarity. In contrast, Zhao and Lu [10] assume that the chemical reaction softens the surface, making it easier for the material to be mechanically removed by particles in the slurry. Similarly, Paik and Park [11] assume that the oxide polishing suspension, which contains abrasive colloidal silica particles, chemically reacts with the specimen's surface. Vibropolishing is described by Brust [12] as a combination of peening, burnishing, and microcutting, whereas Domblesky et al. [13] characterize it as a sequence of randomized grinding processes. By using ultrasonic vibrations, the agglomeration of abrasive particles in the slurry can probably be prevented [14]. Chemical-mechanical polishing is considered the most effective method in the semiconductor industry for surface planarization, such as in the thinning and smoothing of thin films during the production of integrated circuits [10,15]. Vibropolishing is used for

* Corresponding author.
E-mail address: christian.greiner@kit.edu (C. Greiner).

https://doi.org/10.1016/j.matdes.2025.114584
Received 18 April 2025; Received in revised form 21 July 2025; Accepted 13 August 2025
Available online 15 August 2025

fine finishing and deburring, among other industries, in the aviation jet engine sector to polish components, including turbine and fan blades, as well as blisks, to reduce fuel consumption and lower costs [16].

A major motivation for surface smoothing is the enhancement of tribological performance. Improving tribological systems is crucial, as they account for 23 % of global energy consumption, with 20 % specifically used to overcome friction [17]. Optimizing systems like those in vehicles and machinery could result in a reduction of up to 8 % in overall energy consumption. It was found that introducing pores can result in nearly a threefold reduction in friction [18]. Thus, they are highly promising in bringing us closer to the goal of energy reduction. This study hypothesizes that the surface treatment method has a significant impact on the tribological performance, including the long-term behavior of porous copper specimens. Should it prove that, with an appropriate surface treatment, the low coefficient of friction remains stable over a long period, not only could energy consumption be reduced in applications, but time and cost savings could also result from less frequent component replacements.

The influence of pores on the tribological behavior under unlubricated conditions can result in either an increase or a decrease in friction and wear. According to previous work, sintering pores lead to a drastic reduction in the friction coefficient in unlubricated copper, while a higher wear rate is to be expected [18]. Ordoñez et al. [19] found that although a higher sintering porosity in Fe-Mo-C steel leads to an increased wear rate, it also results in a slight reduction of the coefficient of friction. In contrast, Sinha and Farhat [20] showed that an increase in porosity in both aluminum and aluminum alloy 6061 leads to an increase in friction due to enhanced asperity-asperity contact as well as wear due to a porosity induced higher surface roughness and a reduction in hardness. On the other hand, Martin et al. [21] demonstrated that increasing the porosity of stainless steel can improve wear resistance under unlubricated conditions, as they assumed that during the initial stages of sliding, the pores are filled with wear debris and by plastic deformation. Chen et al. [17] showed that nanopores in gold can enhance strength without compromising ductility by trapping dislocations at the nanopores.

Similarly, no general relationship can be established between surface roughness and tribological behavior. While Al-Samarai et al. [22] found that friction increases with higher roughness on aluminum–silicon casting alloys, Kubiak et al. [23] observed that in both carbon alloy (AISI 1034) and titanium alloy (Ti-6Al-4 V), lower friction prevails at high roughness under fretting conditions. Svahn et al. [24] observed, on the one hand, an increase in friction with rising roughness in an amorphous carbon coating containing chromium, whereas, on the other hand, no correlation between friction and roughness was found in an amorphous carbon coating containing tungsten. Liang et al. [25] revealed that an increased roughness on AISI 1045 steel specimens leads to an unstable coefficient of friction with greater fluctuations.

Numerous studies have already investigated the tribological behavior of materials. Bowden and Tabor [26] assumed that the frictional force consists of two components: adhesion and deformation. Due to cold welding and adhesion, junctions form in the real contact area between the specimen and the counterbody. When the counterbody slides over the specimen's surface, a certain force is required to shear off these junctions. The deformation component results from processes like grooving, plowing or cracking of the softer surface caused by the asperities of the harder material. In copper, significant changes in the microstructure have been observed under tribological loading. After 100 sliding cycles, a network of geometrically necessary dislocations forms, creating cell walls and further develops into small angle grain boundaries [27,28]. Ultimately, they evolve into subgrains and are progressively displaced deeper below the surface. These subgrains exhibit grain boundaries aligned parallel to the surface, with grain sizes increasing toward the interior of the material [29]. According to Argibay et al. [30], in pure copper with a low friction coefficient under 0.5, grain sizes of 10–20 nm are present directly below the surface, allowing for shear accommodation through grain boundary sliding. In contrast, for friction coefficients above 0.5, larger grains are observed below the surface, and dislocation-based plasticity occurs. Before grain refinement, tribo-oxidation occurs under tribological loading in air, where amorphous oxides form, particularly at surface defects [31]. Since diffusion is faster at the copper-oxide interface and at Cu_2O grain boundaries compared to in pure copper, oxidation predominantly occurs at the interface, resulting in the formation of island-like clusters [31–33]. With an increasing number of sliding cycles, these clusters grow, forming thermodynamically more stable Cu_2O nanocrystalline domains, and the coalescence of these semispherical clusters results in a continuous oxide layer [31].

If porous copper exhibits long-term stable low friction with the appropriate surface treatment, this could have important implications for component design across various industries. Porous copper components are increasingly relevant in applications that require low weight, high conductivity, and reliable tribological performance, like in aerospace, automotive, and railway industries [34,35]. Their reduced mass due to porosity enables material savings and improved energy efficiency, contributing lower fuel consumption and emissions [36,37]. Moreover, their high thermal and electrical conductivity makes them promising for dynamic applications including bearings, seals, sliding elements, electrical contacts, and heat exchangers involving moving components, provided that the porosity-induced loss of conductivity is not critical compared to the friction reduction achieved [38–40].

Despite their potential, the tribological behavior of porous copper remains insufficiently understood, particularly the interaction of sintering-induced pores with surface treatments and the effects on friction and wear. While porosity offers functional benefits, it creates complex surface topographies that potentially deteriorate tribological performance. Previous studies have largely focused on the tribological behavior of dense copper, leaving a significant knowledge gap on unlubricated porous copper.

This study addresses this gap by systematically investigating the influence of two distinct surface treatment techniques, electropolishing and chemical–mechanical vibropolishing, on the friction and wear of porous unlubricated copper. These methods differ fundamentally in how they affect surface roughness and pore exposure, offering a unique opportunity to tailor tribological performance through surface design. A central innovation of this work is the investigation not only of the direct effects of surface treatments but also the durability of friction reduction over an increased number of sliding cycles, from 1000 to 5000, equivalent to 33.3 h of continuous testing. This approach enables assessment of long-term performance, which is essential for practical applications where stable, low-friction behavior over time is critical. By combining surface engineering with tribological testing, this study provides new insights into how to design functional porous copper components with optimized tribological properties. These findings could support broader use of porous copper in lightweight, energy-efficient systems.

2. Experimental

2.1. Materials

Copper was chosen for this work as it has already been shown that introducing porosity can reduce the friction coefficient by more than 50 % [18]. Building on this, the present study investigates the effect of surface treatment on the frictional behavior of porous copper. Furthermore, numerous studies on the tribological behavior of copper under mild loading conditions are already available, which enables a better understanding of the results of this study and allows conclusions to be drawn. In addition, copper is characterized by its high electrical and thermal conductivity, as well as its ductility, contributing to uniform heating and improved densification of the powder particles during the sintering process [41,42]. For the investigations of this study, two types of copper powder with a purity of 99.95 % and d90 particle sizes of 20

μm and 36 μm from Inopowders S.A.S, Paris, France, were used. The powder was maintained in an argon atmosphere to reduce oxidation. Tribological tests were performed with a 10 mm diameter single-crystal sapphire sphere supplied by SaphirwerkAG, Bruegg, Switzerland.

2.2. Sample fabrication

Different specimens were produced, varying in pore quantity and size. While the finer powder was used for the specimens with small pores, the coarser powder was employed for those with large pores. In order to investigate the effect of surface preparation, two specimens with many small pores (MSP) were produced using Field Assisted Sintering Technology (FAST). To study the impact of an increase in cycles on the development of the microstructure, a specimen with few small pores (FSP), as well as an MSP sample and a specimen with many big pores (MBP), were fabricated. The FAST technique was performed with a HP D 25/1 from FCT Systeme GmbH, Frankenblick, Germany. Initially, a graphite die, lined with a graphite foil and having a diameter of 20 mm, was filled with powder to a height of 3.4 mm. Following this, the powder was pre-compacted using a force ranging from 3 to 5 kN. At the beginning of the FAST process, the specimens were loaded with 5 kN and a vacuum was applied for up to 3 min, resulting in a final pressure of less than 1 mbar. In the second step, the chamber was flooded with argon for 45 s, followed by redrawing the vacuum for 1 min. Afterwards, the specimens with many sintering pores were continuously subjected to a 5 kN load for 1.5 min, while the load on the specimens with few pores increased to 15.7 kN during this time interval. Subsequently, the samples were heated until 450 °C was reached, using a maximum heating power of 21 kW, resulting in a heating rate of around 140 K min^{-1}. Throughout the process, a pulsed current was applied with a pulse duration of 25 ms and a 5 ms pause. After reaching 450 °C, the specimens were heated to 600 °C within 1.5 min by applying a heating rate of 100 K min^{-1}. This maximum temperature was maintained for 2 min before cooling the specimens at a rate of 100 K min^{-1}. Upon reaching 400 °C, the specimens initially loaded with 15.7 kN were gradually unloaded to 5 kN over 1 min, while those with lower loading were kept at 5 kN. After venting the chamber and waiting for 7 min, it was opened. Finally, after a 5 min waiting period, the die had cooled to room temperature and was removed.

2.3. Sample preparation

Following the FAST process, the specimens were ground with SiC papers, reaching a grit size of 4000 with the grinding machine Saphir 320, both from QATM GmbH, Mammelzen, Germany. Subsequently, the specimens were polished using MD-Dur polishing cloths and a LaboPo-30, both from Struers GmbH, Fellbach, Germany, with 3 μm and 1 μm diamond suspensions supplied by Cloeren Technology GmbH, Wegberg, Germany. Afterwards, the samples underwent either a chemical–mechanical vibropolishing or an electropolishing step. During the 15 h vibropolishing process, the specimen was polished with an OP-U non-dry solution from Struers GmbH, Fellbach, Germany, using a VibroMet 2 from Buehler, Lake Bluff, Illinois, United States, at an amplitude of 60 %, on a MicroCloth polishing cloth from Buehler ITW Test and Measurement GmbH, Leinfelden-Echterdingen, Germany. The specimen preparation was completed by cleaning it with detergent and deionized water, and was finished with a final rinse using isopropanol. During electropolishing, 2 cm^2 of the specimen was polished for 20 s with a voltage of 28 V and a flow rate of 16, using the LectroPol-5 electropolishing device and the D2 electrolyte from Struers GmbH, Fellbach, Germany. Immediately after electropolishing, the sample was rinsed with 200 ml of deionized water and then ultrasonic cleaned in isopropanol for 10 min. Before fixing the sample in the tribometer, it was dried using an air blower.

2.4. Tribological testing

In order to conduct the tribological tests, the specimens were mounted on a precision linear stage (M−404.2DG from Physik Instrumente (PI) GmbH & Co. KG, Karlsruhe, Germany). A piezoelectric, three-axis force sensor (type Z16758 from Kistler Instrumente AG, Winterthur, Switzerland) was used to measure the friction throughout the tests. The spheres were aligned using a light source and a polarizer, ensuring that the contact surface was parallel to their hexagonal close-packed crystal basal plane. During the entire tribological tests, the spheres were loaded with a 2 N force using a dead weight, and they slid over a distance of 6 mm at a speed of 0.5 mm s^{-1} for 1000 or 5000 reciprocating cycles across the middle of the sample surfaces, corresponding to either the bottom or top faces of the cylindrical specimens. All tribological tests were performed at room temperature and in air with a controlled relative humidity of 50 %. Immediately after the last stroke, the specimens were unloaded and stored under vacuum to prevent oxidation.

2.5. Subsurface microstructure characterization

Following the tribological tests, the samples were thoroughly examined in order to understand their tribological performance and to analyze the impact of the surface preparation methods. To achieve this, cross-sections were cut using a focused ion beam (DualBeam Helios NanoLab 650 from ThermoFisher Scientific, Waltham, Massachusetts, United States). The cross-sections were prepared parallel to the sliding direction, at the center of the wear tracks. In order to protect the surface to be investigated from the cutting ion beam, one platinum layer was deposited using the electron beam and a second one was applied with the ion beam. Imaging of the microstructure was conducted in immersion mode, using a current of 0.8 nA and an acceleration voltage of 2 kV.

2.6. Surface characterization

Surface analysis was performed using light microscopy images (BX60 from Olympus, Tokyo, Japan), scanning electron microscopy (SEM) images (Helios 650), and optical surface profilometry images. While the wear track profiles of the chemical–mechanical vibropolished specimens after 1000 cycles were measured with the optical surface profilometer Plμ Neox from Sensofar, Barcelona, Spain, the chemical–mechanical vibropolished surface, the wear track profiles after 5000 cycles, and the electropolished specimen were evaluated with TopMap Micro.View + from Polytec GmbH, Waldbronn, Germany, using a 10x magnification objective from Nikon, Tokyo, Japan. The images were acquired at the center of each wear track. The height profiles of the various wear tracks shown in this study represent the average values along the sliding direction across a 0.9 mm distance. To compare the roughness, the arithmetic means of the height, given by

$$S_a = 1/A \iint |z(x,y)| \, dxdy \quad (1)$$

were calculated using the ordinate values z(x,y) within the evaluation area A, according to ISO 25178–2:2021. Microhardness measurements were performed using a FISCHERSCOPE® H100 from Helmut Fischer GmbH, Sindelfingen, Germany, equipped with a Vickers indenter. A test load of 250 mN was applied, and five indentations were made per sample.

2.7. Density measurements

The specimen densities were measured using the Archimedes method. To ensure the reliability of the water density value, a thermometer was immersed in deionized water 2 h before measuring the weight using a precision balance (type R160P-*D1 from Sartorius AG, Göttingen, Germany). The sample density

$$\rho_S = m_{S(A)}/(m_{S(A)} - m_{S(W)})\cdot(\rho_W - \rho_A) + \rho_A \quad (2)$$

was calculated with the densities of water ρ_W according to ISO 15212–1:1998 and air $\rho_A = 0.0012$ g cm^{-3}, after weighing the samples in air $m_{S(A)}$, as well as in water $m_{S(W)}$ [43]. All measurements were repeated three times, with values read exactly after 5 min and the average of these readings was used to calculate the sample density. For determining the relative density of the samples, the absolute density of copper was assumed to be 8.96 g cm^{-3} [44].

3. Results

3.1. Chemical-mechanical vibropolishing vs. Electropolishing

Initially, the densities of the ground specimens were measured. The MSP specimen that was subsequently electropolished had a total density of 85.0 %, while the MSP specimen that was vibropolished afterward showed a total density of 84.8 %. After being electropolished, or respectively vibropolished, the surfaces of the specimens were analyzed using both the profilometer and SEM, as shown in Fig. 1. It was found that the vibropolished specimen had a S_a value of 0.11 µm, while the electropolished sample had a value of 1.63 µm, more than 16 times higher. In both the profilometer and SEM images, it is evident that electropolishing significantly enlarged the sintering pores and led to rounding of the sintering pore edges. In comparison, vibropolished FSP and MBP yielded even lower average Sa values of 0.03 µm and 0.04 µm, respectively. SEM images presented in Fig. S1 highlight the distinct surface characteristics of the different specimen types. Clear differences between the sample types and surface preparation methods are also evident in the hardness values. While the vibropolished FSP sample show an average microhardness of 68 HV, MBP 41 HV, and MSP 49 HV, the electropolished MSP sample exhibit a significantly lower average hardness of 31 HV, as shown in Fig. S2.

A closer examination of the electropolished surface in the SEM, shown in Fig. 2, revealed circular patterns on the surface, which were visible at varying densities in different areas of the specimen. In the center of the circular patterns small craters could be detected, as visible in Fig. 2c). It could also be observed that electropolishing resulted in a more pronounced material removal at the grain boundaries.

After conducting the tribological experiments, SEM investigations in Fig. 3, particularly in the secondary electron (SE) images in Fig. 3a) and b), reveal that delamination occurred on the surface during both tests. The craters within the wear tracks resemble the sintering pores adjacent to the tracks, which were enlarged by the electropolishing process. Backscattered electron (BSE) images in Fig. 3c) and d) show that these sintering pores were partially worn away and filled during tribological loading, especially at the center of the wear tracks.

Similarly, no significant differences in the subsurface microstructure could be observed in Fig. 4 between the specimen tested immediately after electropolishing and after an additional 24 h exposure to air before the tribological test. In both microstructures, the subsurface deformation layer in Fig. 4a) and c) is similarly pronounced, with a depth of 3.8 µm after electropolishing and 7.4 µm with an additional 24 h after electropolishing. Also, the dark gray zone in Fig. 4b) and d) is similarly developed, with a depth of 1.6 µm after electropolishing and 0.8 µm tribologically tested 24 h after electropolishing. In this zone, black elongated features are visible in both microstructures. Additionally, the sintering pores seem to act as boundaries for the subsurface deformation, as the grain refinement does not extend deeper into the material once a sintering pore appears.

Based on the mean wear track profiles measured from white light interferometric images in Fig. 5, it can be observed that the electropolished samples exhibited a much rougher surface compared to the vibropolished ones. Additionally, for the sample with few sintering pores, pile-ups can be observed at the sides of the wear track, in contrast to the specimens with more sintering pores. In general, the wear tracks of MSP show a tendency to be, on average, 0.9 µm less deep and 100 µm narrower than those of MBP. The wear track depths of the electropolished MSP lie between the depths of vibropolished MSP and MBP.

Light microscopy images in Fig. 6 show no difference between the wear track width of the MSP surface that was tribologically tested immediately after electropolishing in Fig. 6a) and the wear track of the

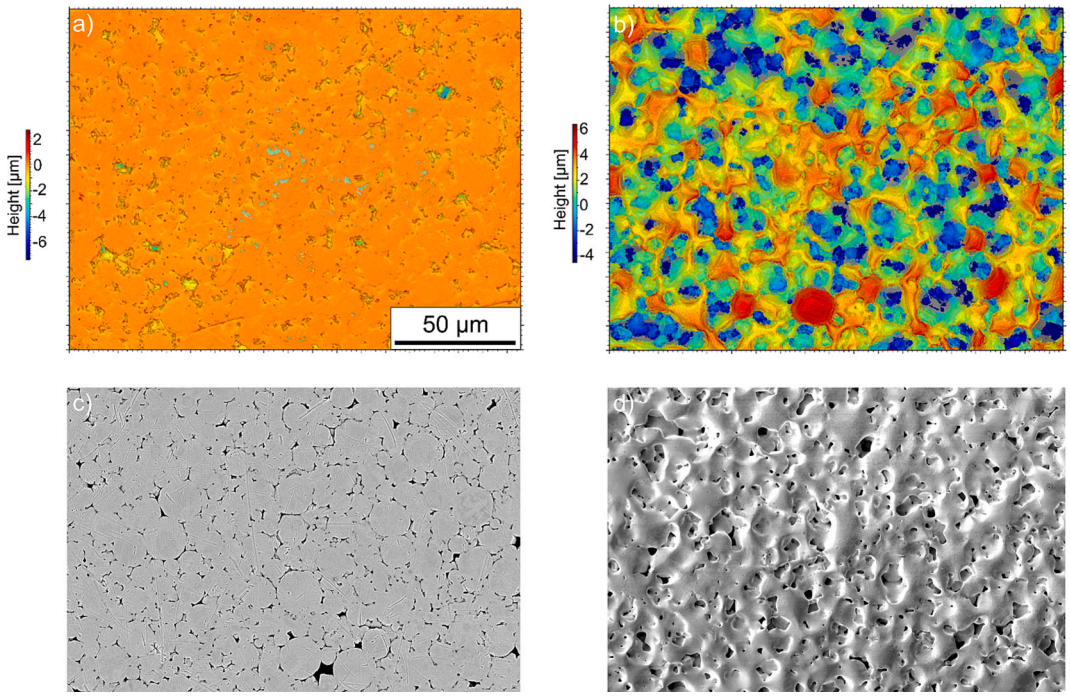

Fig. 1. Optical surface profilometry images of the a) vibropolished and b) electropolished specimen surfaces with a similar overall porosity, and scanning electron microscopy (SEM) images of the c) vibropolished and d) electropolished surfaces. The scale bar in a) applies to all images. In contrast to vibropolishing, electropolishing led to an enlargement of the sintering pores at the surface and rounding of their edges.

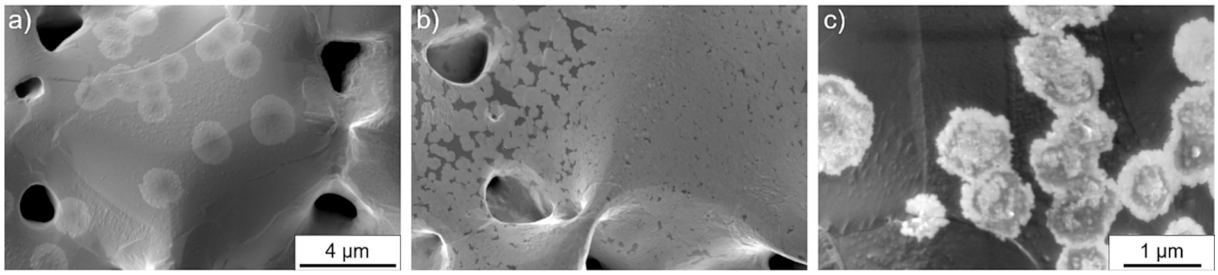

Fig. 2. SEM images of the electropolished surface showing circular patterns at varying densities, with a) and b) taken from different spots in the center of the specimen. The scale bar in a) applies to both a) and b). At a higher magnification in c), it can be seen that small craters are present in the center of the circles.

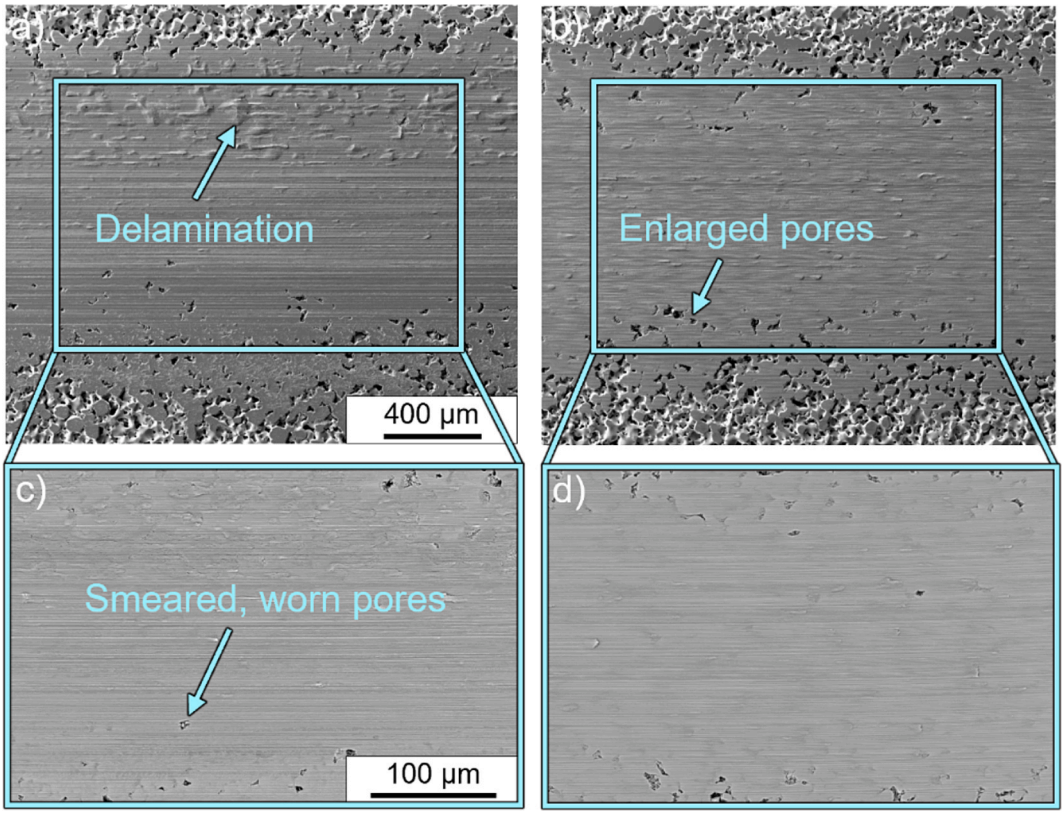

Fig. 3. SEM images of the wear tracks of the surface with many small pores (MSP) directly after electropolishing in a) and c) as well as after being exposed to air for 24 h in b) and d). While secondary electron (SE) images with the same scale are shown in a) and b), enlarged backscattered electron (BSE) images are visible in c) and d) using the same scale. Both SE images show delamination and enlarged sintering pores at the edges of the wear tracks, while BSE images reveal partially filled and worn sintering pores towards the center.

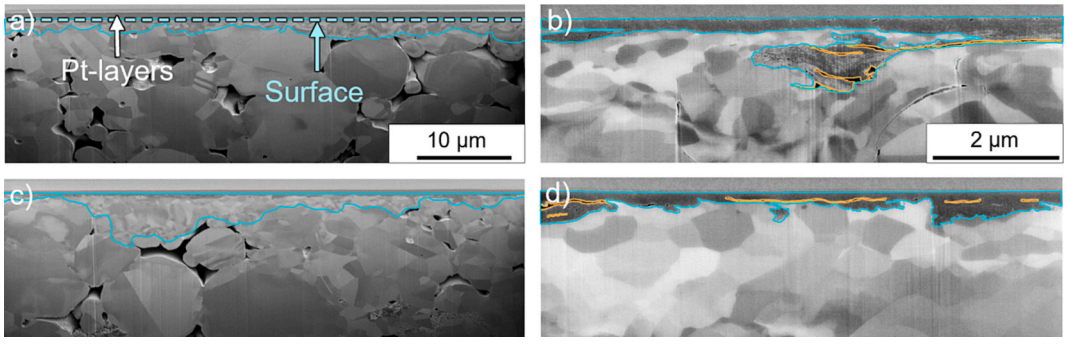

Fig. 4. Cross-section images in sliding direction at the center of the wear track for the MSP specimen tested directly after electropolishing in a) and b), and after an additional 24 h air exposure in c) and d). In a) the specimen surface is marked exemplarily beneath the protective platinum layers. The subsurface deformation layer, highlighted in blue in a) and c) using the same scale, is similar in both microstructures, as is the dark gray zone marked in blue and the elongated black features emphasized in orange in b) and d), which also use the same scale.

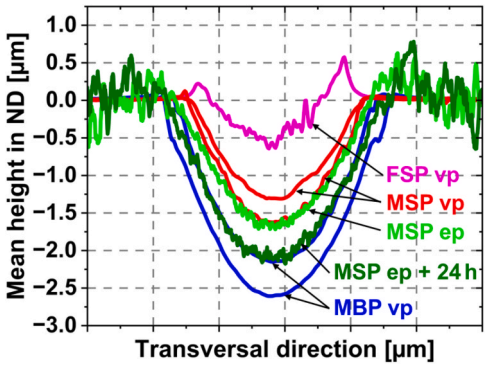

Fig. 5. Wear track profiles based on white light interferometric images show that samples with many sintering pores exhibit no significant pile-ups, unlike the specimen with few small pores (FSP). The vibropolished (vp) specimen with many big pores (MBP) exhibit deeper and wider wear tracks than the vp MSP one, while the electropolished (ep) MSP sample falls in between, with a rougher surface than the vp ones.

surface exposed to air for 24 h before the tribological test in Fig. 6b). Additionally, both exhibit a similar groove pattern in sliding direction, as well as the same grayish discoloration in the wear track. In both, craters can be detected, which are more frequent at the edges of the tracks.

The coefficients of friction of the varying specimen types over 1000 cycles in Fig. 7 exhibit significant differences between electropolished and vibropolished MSP. While the coefficient of friction of the vibropolished sample reaches a value of 0.2 after just a few cycles and shows only a slight increase over the cycles, the coefficient of friction of the electropolished sample reaches nearly three times that value within the first 50 cycles. The value for the sample tested directly after electropolishing subsequently drops by 0.1 and then rises, reaching the value of the first peak after approximately 600 cycles, whereas the coefficient of friction of the surface exposed to air for 24 h after electropolishing shows a steady, slight increase. After 1000 cycles, the coefficients of friction of the electropolished MSP sample are comparable to the one of vibropolished FSP, ranging between 0.6 and 0.65. Thus, these coefficients of friction are about 2.5 times higher than that of vibropolished MSP, which reaches a value of approximately 0.25 after 1000 cycles.

3.2. 1000 vs. 5000 cycles

By increasing the number of cycles from 1000 to 5000 of the vibropolished specimens, it can be observed in Fig. 8a) that the differences in the coefficients of friction due to varying porosities remain. The friction coefficients of MSP and MBP stabilize at a value of 0.23 after 5000 cycles, while the friction coefficient of FSP is nearly three times higher, reaching 0.67. The increase in the coefficient of friction of MSP after approximately 2500 cycles can be attributed to an increase in relative humidity, as shown in Fig. S3 in the supplementary information. Fig. 8b) demonstrates that neither the width nor the depth of the wear tracks changed with an increase in the number of cycles for any of the specimen types. Specimens with many sintering pores continue to exhibit no pile-ups at the edges of the wear track after 5000 cycles. In contrast, FSP shows pile-ups after both 1000 and 5000 cycles.

Below the surfaces of the different specimen types after 5000 cycles, a zone with finer grains is observed with the help of cross-section images in Fig. 9a), c), and e). This zone is approximately 15.8 µm deep for FSP, while for specimens with many sintering pores, it is much shallower, measuring 0.8 µm for MSP and 1.2 µm for MBP. In all three microstructures a dark gray layer appears, as visible in Fig. 9b), d), and f). This layer is significantly more pronounced in FSP, as it extends up to 1.9 µm beneath the surface, while for MSP it reaches 0.3 µm and for MBP 0.5 µm. In contrast to the other microstructures, FSP exhibits black elongated features beneath the surface, as shown in Fig. 9b).

4. Discussion

To answer the leading question of this manuscript – *How surface treatment of porous copper samples dictates dry friction and wear?* – both the influence of surface preparation on the tribological performance and the

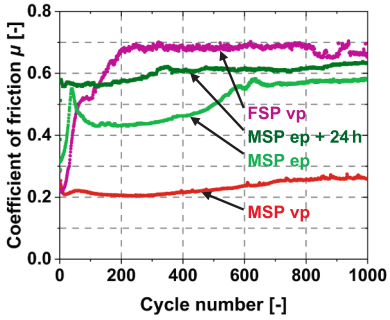

Fig. 7. Coefficients of friction of the different specimen types over the 1000 sliding cycles. It can be observed that, in contrast to the vibropolished (vp) MSP sample, the friction coefficients of the electropolished (ep) MSP specimen increase significantly within the first 50 cycles, similar to the vp FSP one.

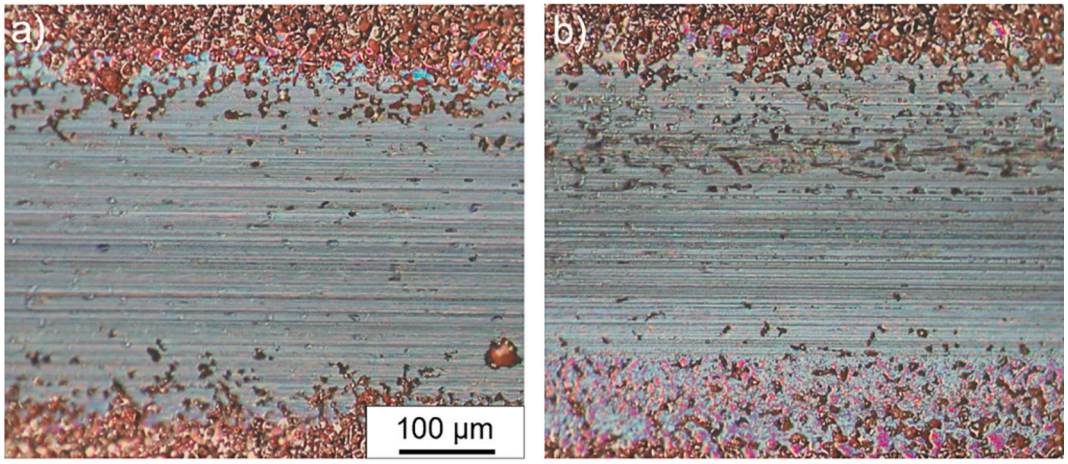

Fig. 6. Light microscopy images of the wear tracks of the MSP specimen tested a) directly after electropolishing and b) after additionally exposed to air for 24 h. The scale in a) applies to both images. Both show a similar color and width, along with small craters and grooves in sliding direction.

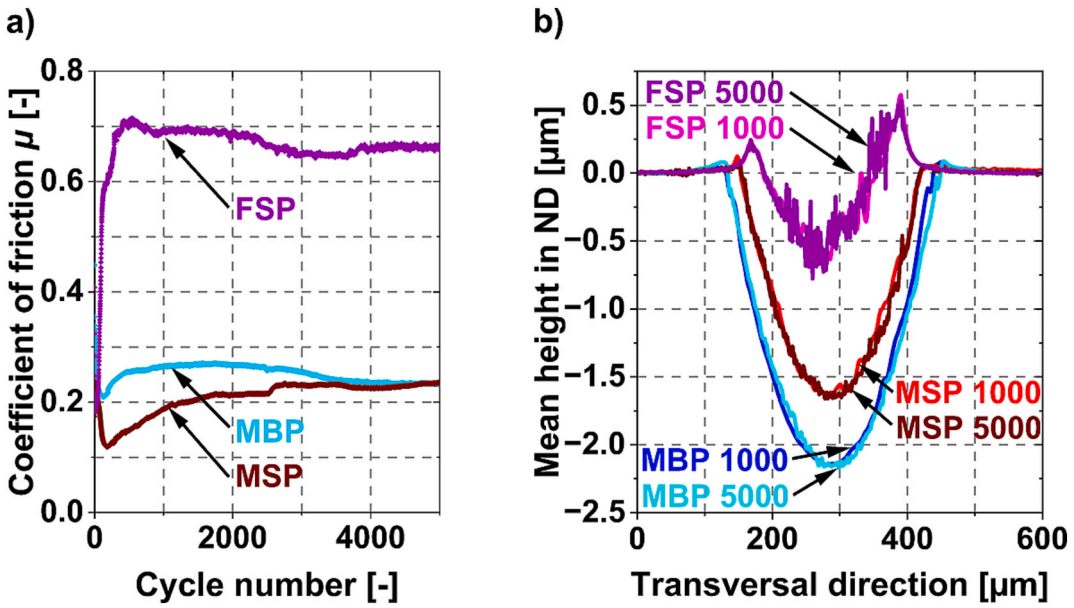

Fig. 8. A) development of the coefficients of friction over 5000 cycles for vibropolished FSP, MSP and MBP specimens, and b) comparison of their wear track profiles based on white light interferometric images after 1000 and 5000 cycles. Both the coefficients of friction and the wear track profiles show no significant change with the increasing number of cycles. The coefficients of friction of the specimens with many sintering pores seem to stabilize at a consistent value after 5000 cycles.

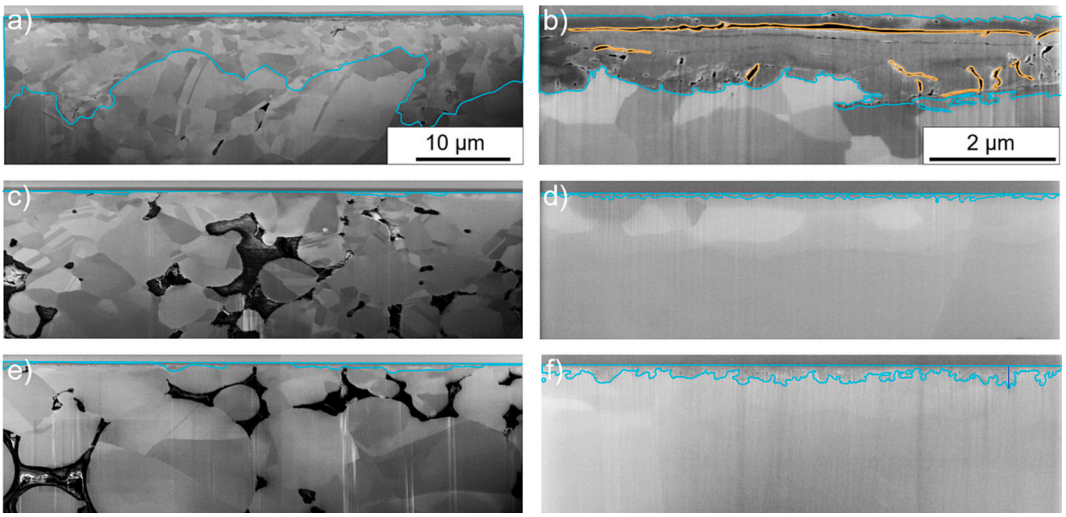

Fig. 9. Cross-section images in sliding direction at the center of the wear track after 5000 cycles of the vibropolished FSP specimen in a) and b), MSP in c) and d), MBP in e) and f). The subsurface deformation layers of the different specimens are highlighted in blue in a), c) and e), with the scale in a) applying to the three images. In b), d), and f), the dark gray zones beneath the surfaces are outlined in blue, while the black, elongated features in this zone are marked in orange. The scale in b) applies to these images. Specimens with many sintering pores exhibit both a significantly lower subsurface deformation compared to FSP, as well as smaller dark gray zones and no black elongated features.

long-term effectiveness of friction reduction of the tribologically more beneficial method, through a significant increase in loading duration, were investigated.

4.1. *Chemical-mechanical vibropolishing vs. Electropolishing*

First, the influence of surface preparation was investigated by comparing the effect of chemical–mechanical vibropolishing and electropolishing of the MSP specimens. By vibropolishing, the preparation-induced Beilby layer and scratches could be reduced [45]. Additionally, after being smeared during preparation, as seen in Fig. S4a) in the supplementary information, the sintering pores between the particles were exposed during vibropolishing, as shown in Fig. 1a) and c). Under the assumption, according to Steigerwald et al. [9], that clusters of atoms are first removed from the surface and secondly chemically dissolved, the remaining scratches after vibropolishing, visible in Fig. 1c), can either be attributed to insufficient chemical reaction, causing the clusters to scratch the sample surface, or to dissolved particles that may have been trapped in the sintering pores. The latter is confirmed by small particles exposed in the sintering pores after vibropolishing, as shown in Fig. S4b). Electropolishing of the MSP specimen not only resulted in the removal of the Beilby layer and scratches, as well as the exposure of the sintering pores but also caused an enlargement of the sintering pores, visible in Fig. 1b) and d), due to a higher current density in the pores, which led to increased material removal [46]. As noted by Yang et al. [1], the current density is highest at sharp edges, which explains the observed rounding of the sintering pore contours during electropolishing. Both led to a significant increase in roughness,

compared to the vibropolished surface. Since similar overall porosities were measured for the two MSP specimens, which were subsequently either vibropolished or electropolished, the porosity affected the effective Young's modulus of both specimens to the same extent. According to Buch and Goldschmidt [47], a porosity of 15 % is expected to result in an effective Young's modulus of 98 GPa. Fig. S2 shows that the average microhardness of the vibropolished MSP is higher than that of the electropolished one. According to Fellah et al. [48], the effective Young's modulus increases with hardness. Campbell et al. [49] detected local variations in the effective Young's modulus through nano-indentation; however, no change in the average effective Young's modulus could be experimentally determined due to surface roughness. Accordingly, Fig. S2 reveals a greater scatter of hardness measurement values in the electropolished MSP sample compared to the vibropolished one, indicating local differences in the effective Young's modulus. Therefore, it is plausible to assume that the overall average effective Young's modulus of the electropolished and vibropolished specimens are the same. Considering porosity and surface roughness in the calculation of the maximum Hertzian pressure, a value of 507 MPa could be expected in both specimens during the tribological tests [50]. However, due to the enlarged sintering pores on the surface of the electropolished specimen, as shown in Fig. 1, the contact area between copper and the sapphire sphere was smaller at the beginning of the tribological test compared to the vibropolished specimen. Consequently, the applied load from the sphere was distributed over a smaller contact area in the electropolished specimen, so that a higher maximum pressure was expected compared to the vibropolished one, since surface roughness, just like the predominant plastic deformation, is not considered in the calculation of the maximum Hertzian pressure. This surface-induced stress increase caused more pronounced plastic deformation beneath the surface, as shown by the grain refinement in Fig. 4, compared to the shallower layer seen in the vibropolished MSP specimen, as reported by Lung et al. [18]. This increased deformation is also evident in both the light microscope images in Fig. 6 and the SEM images in Fig. 4. Specifically, grooves in the sliding direction, which are a typical feature of abrasive wear, could be observed [51]. The asperities of the harder sapphire sphere penetrated and cut the softer copper specimen. In the wear tracks of the vibropolished MSP sample, on the other hand, these grooves were barely found, as little subsurface deformation occurred [18]. Another indication, particularly evident in the BSE images in Fig. 3, is that in the center of the wear track, where, according to the Hertzian pressure distribution, the stress is highest during the tribological tests, the sintering pores have been either smeared or removed [52]. In contrast, after the tribological loading, the sintering pores in the vibropolished MSP specimen remained almost unchanged at the surface, which supports the fact that no significant subsurface deformation was observed. Through the reduction of sintering pores in the contact area of the electropolished specimens and the enhanced depth in the mean height profile of the wear track, as shown in Fig. 5, the contact area between the specimen and the sapphire sphere increased. While this contributed to a reduction in the maximum stress, as the force from the sphere was distributed over a larger real contact area, the overall shear force increased since, according to Bowden and Tabor [26], a higher amount of junctions were formed and sheared in the larger real contact area of the specimen and the sphere, resulting in an increase in the coefficient of friction [53].

Upon examining the mean height of the wear track profiles in Fig. 5, it is evident that the surface of the electropolished MSP sample is significantly rougher than that of the vibropolished MSP specimen, due to the previously described enlarged sintering pores, delamination and grooves in the sliding direction. Additionally, both the electropolished and vibropolished MSP specimen do not show pile-ups on the sides of the wear tracks, unlike the FSP sample. While in the vibropolished MSP specimen, particles were pressed down into the subsurface sintering pores, in the electropolished MSP sample, material was removed and plowhed into the enlarged surface sintering pores, especially in the center of the wear tracks. Plowing takes place when one surface is significantly harder than the other, leading the asperities of the harder surface to forcibly displace the softer material to a substantial depth beneath the surface [54]. Similar to the electropolished MSP sample, in the vibropolished FSP specimen, material was pushed onto the sides of the wear track. However, due to the lack of sufficient sintering pores to fill, pile-ups formed along the edges of the wear track. Fig. 5 also shows that, depending on the location on the sample where the tribological tests were conducted, the wear tracks exhibited varying widths and depths. This is attributed to the position of the sintering pores on and below the surface as well as the sintering pore density. Therefore, a sample-dependent variance in the wear track depth within the same specimen is generally expected. Consequently, the different depths of the wear tracks, from the tribological experiments conducted immediately after electropolishing and 24 h later, cannot be attributed to the aging time, including the presence of a native oxide layer after 24 h in air, which is reported by Platzman et al. [55] to be between 2.5 and 4.0 nm thick, and by León et al. [56] to be around 2 nm thick. However, it is generally observed that the width and depth of the wear tracks are greater in the vibropolished MBP specimen, as particles were more easily pressed into the larger sintering pores [18]. While the average depth of the wear tracks in the electropolished MSP specimen lies between that of the vibropolished MSP and MBP samples, their width is almost identical to that of the MBP sample. This could be due to the fact that the sintering pores were significantly enlarged during electropolishing compared to those in the vibropolished MSP sample, thus behaving more similarly to the MBP specimen.

In addition to the deformation, the dark grey zone immediately beneath the surface, visible in Fig. 4b) and d), is of significance, representing the tribo-oxidation zone according to Rau et al. [57]. Due to the deformation-induced grain refinement shown in Fig. 4a) and c), the tribological loading led to the formation of numerous new dislocations and grain boundaries through the rearrangement of dislocations during dynamic recovery, both serving as diffusion paths for oxygen [57–59]. Since the vibropolished MSP specimen exhibits only a very small tribologically induced subsurface deformation layer, the tribo-oxidation zone is correspondingly less pronounced than in the electropolished specimen, with a depth of 0.1 μm.

During the tribological tests Kirkendall pores form between the tribo-oxide and copper because copper ions diffuse faster than oxide ions [57,60]. With progressing oxidation, pores form along the diffusion paths, leading to the formation of cracks beneath the surface, which result in delamination at the surface [57]. Other factors contributing to delamination could include the higher hardness of copper oxide, which leads to a greater tendency for crack formation compared to copper, as well as dislocation pile-up at the copper-oxide interface [31,61,62]. Since the tribo-oxidation zone is significantly more pronounced in the electropolished MSP specimen compared to the vibropolished MSP sample, cracks within the tribo-oxide and delamination at the surface are observed in the wear track of the electropolished specimen, as visible in Fig. 4b) and d). Both the depth of subsurface deformation and the development of the tribo-oxidation zone, along with cracks beneath the surface, are similar in the electropolished MSP and the vibropolished FSP specimens [18].

The spots, visible in Fig. 2, are likely due to the effects of the electrolyte. According to Jurin's law, the capillary force is inversely proportional to the diameter of the capillary tube [63]. Therefore, a high capillary force is expected in very small craters, as observed in Fig. 2c). Neither rinsing with water nor the ultrasonic cleaning with isopropanol could probably flush out the electrolyte from the small cavities. After drying the surface, a subsequent pressure difference between the outside and the inside of the small craters could cause the liquid to rise within the small craters and eventually emerge at the surface over time. This phenomenon of rising liquid was observed a few minutes after drying the MSP specimen, which had been previously cleaned with isopropanol. The electrolyte consists of ethanol, propan-1-ol, and

phosphoric acid. As ethanol and propan-1-ol could evaporate at the surface, the concentration of phosphoric acid increased, leading to supersaturation, which most probably resulted in crystallization around the craters, forming round spots visible in Fig. 2 [64,65]. Furthermore, in combination with water, phosphoric acid can form crystalline hemihydrates at room temperature [65–67]. In addition to crystallization due to supersaturation, crystallization could also occur due to reactions with water, with which the specimen was rinsed to stop the reaction after electropolishing, or with humid air during the tribological tests. This crystallization at the surface could affect the tribological tests. During the experiment after 24 h, the proportion of crystallization spots was likely significantly higher than in the first experiment, directly after electropolishing, where crystallization likely occurred mainly during the tribological test. Additionally, as shown in Fig. 2a) and b), the number of these spots varied across the surface. Since the sapphire sphere was probably not only in contact with copper or its oxides in these areas, but also with crystallized phosphoric acid, among other substances, this could influence the coefficient of friction.

The differences in the coefficient of friction curves between the experiment conducted immediately after electropolishing and the one performed 24 h later, as shown in Fig. 7, are likely not caused by the native oxide layer present in the latter. It has already been shown that even with the same exposure time to air before the tribological experiment and under identical experimental conditions, different running-in behaviors of the coefficients of friction could be observed, with the steady-state coefficients of friction sometimes only being reached after 500 cycles [68,69]. It was also demonstrated that different exposure times to air, up to 56 h, have no influence on the steady-state coefficient of friction [69]. Whether the crystallization of phosphoric acid on the surface has an impact on the coefficient of friction would need to be investigated; however, it seems to have no influence. The progression of the coefficient of friction over 1000 cycles for the different specimens indicates that due to the electropolishing of the MSP sample and the associated phenomena, the coefficient of friction increased by a factor of 2–3 compared to the vibropolished MSP specimen.

Upon examining these findings, it can be concluded that a pronounced subsurface deformation, which was observed in both the specimens with few sintering pores and the electropolished MSP, could accelerate tribo-oxidation and thus the formation of pores, cracks, and delamination on the surface [18]. These energy dissipation mechanisms were associated with an increased coefficient of friction. Since the vibropolished specimens with many sintering pores showed minimal subsurface deformation after 1000 cycles, the tribo-oxidation layer was only slightly developed, and no cracks or delamination were observed. This raised the question: Could a significant increase in the number of cycles lead to the formation of a sufficiently thick tribo-oxidation layer in vibropolished specimens with many pores, despite low subsurface deformation, such that pronounced pores in the tribo-oxide, cracks, and delamination appear, and thus an increase in the coefficient of friction?

4.2. 1000 vs. 5000 cycles

An increase in the number of cycles from 1000 to 5000 resulted in neither a change in the coefficient of friction nor a deepening or widening of the wear tracks of the vibropolished FSP, MSP and MBP, as shown in Fig. 8 and Fig. S5 in the supplementary information. During the tribological loading, the wear rate decreased due to both the increase in contact area with the growing wear track depth, which reduces the maximum surface stress, and the filling of the unevenness on the sapphire sphere, which causes abrasive wear, with the softer copper or copper oxide [51]. Another reason for the wear track depth approaching an equilibrium state, is the hardening of the material due to, among other factors, Hall-Petch strengthening and work hardening. Oxygen can continue to diffuse into the material along the continuously forming dislocation and grain boundary pathways, leading to the progression of tribo-oxidation, without a further increase in the wear track depth. This can be confirmed by a comparison of the subsurface deformation and tribo-oxidation layers after 5000 cycles in Fig. 9 with the microstructures after 1000 cycles, as shown by Lung et al. [18]. It can be observed that there was no change in the subsurface deformation depth, while the tribo-oxidation depth increased. Although the depth of the tribo-oxidation zone in the MBP after 5000 cycles is similar to that of the FSP after 1000 cycles, the oxide is more dispersed and seems non-continuous [18]. Since neither cracking in the tribo-oxide nor delamination at the surface occurred in either the MSP or MBP, the density of the oxide likely plays a significant role in the formation of these energy dissipating phenomena. Fig. 9 further illustrates that the increasing tribologically induced oxidation of the FSP led to the formation of cracks in the tribo-oxide and delamination at the surface after 5000 cycles. This delamination is also visible in the SE images of the wear tracks in Fig. S6 in the supplementary information. These phenomena were not observed after 1000 cycles [18]. FBP, on the other hand, already exhibited cracks and delamination at the surface after 1000 cycles, due to the increased surface stress caused by the larger sintering pores. In all likelihood, this led to a higher tribologically-induced dislocation density and amount of grain boundaries, consequently creating more diffusion channels for oxygen. After 5000 cycles, the depth of the tribo-oxide layer of FSP was similar to that of FBP after 1000 cycles.

These results provide the answer to the central question of this manuscript regarding how the surface treatments influence the tribological properties of porous copper under dry conditions: In the first part, it was demonstrated that electropolishing the specimen before tribological testing destroyed the friction-reducing effect of the sintering pores. Electropolishing induced a significant enlargement of the sintering pores, resulting in higher stresses at the surface during the tribological experiments compared to vibropolished samples. This caused greater plastic deformation, which in turn led to an expanded tribo-oxidation zone, in which cracks formed, resulting in delamination at the surface. Consequently, the electropolishing of a specimen with many sintering pores led to a behavior similar to that of vibropolished specimens with few sintering pores, resulting in a similar trend of the coefficient of friction. Since this differing behavior can be attributed to a varying degree of subsurface deformation, the second part of this study tested whether, even with minimal subsurface deformation in vibropolished samples with many sintering pores, the tribo-oxidation could progress with an increase in the cycle number from 1000 to 5000, to the extent that the tribological behavior would resemble that of vibropolished specimens with few sintering pores or electropolished samples with many sintering pores. After 5000 cycles, no changes were observed in the vibropolished MSP and MBP specimens, either on or beneath the surface, aside from the progression of tribo-oxidation. However, an increase in cycles led to cracks in the tribo-oxide and delamination at the surface in the vibropolished FSP sample, which shows that, with increasing tribo-oxidation, these phenomena eventually emerge. For specimens with many sintering pores, a significant increase in cycles would likely be necessary for this to occur. Future studies could investigate how copper with many and few sintering pores, both vibropolished and electropolished, behaves in lubricated contacts. It could also be interesting to investigate how variations in the tribological conditions, such as a significant increase in load or changes in sliding speed, affect the tribological behavior of specimens with many and few sintering pores.

5. Conclusion

This study examines the effect of surface treatment on the tribological behavior of porous copper under unlubricated conditions. To explore this, specimens with varying pore sizes and densities were sintered and subjected to tribological testing, where a sapphire sphere was moved over a distance of 6 mm at the center of the specimens with a speed of 0.5 mm s^{-1} and a normal force of 2 N for 1000 or 5000 reciprocating cycles. The resulting wear tracks were investigated using

white light interferometry and light microscopy, while subsurface microstructures were analyzed through scanning electron microscopy and focused ion beam cross-sections. The specimen densities were measured using the Archimedes method. It was found that the surface treatment has a significant impact on the tribological behavior, to the extent that the positive effect of the sintering pores, which can reduce the coefficient of friction by more than 50 %, is eliminated. Thus, with proper surface preparation, specimens with high porosity exhibit very stable and low coefficients of friction over a test duration of 33.3 h. In order to reach to this main conclusion, the first part of this study compared the tribological behavior of vibropolished and electropolished specimens and the following main differences were found:

i) Electropolishing caused enlargement of the sintering pores leading to a higher surface roughness with a Sa of 1.63 μm compared to 0.11 μm for the vibropolished sample. Due to the enlarged pores, the electropolished specimen exhibited a smaller contact area with the sapphire sphere during the tribological experiment, which, assuming a maximum Hertzian pressure of 507 MPa in both specimens, resulted in a higher maximum stress in the electropolished sample. Consequently, significantly greater plastic deformation was observed on and beneath the surface of the electropolished specimen compared to the vibropolished one, as evidenced by more pronounced grooves in the sliding direction, as well as smeared and removed surface sintering pores, along with deeper wear tracks and a stronger grain refinement beneath the surface.
ii) More pronounced tribo-oxidation occurred in the electropolished specimen, with a depth between 0.8 and 1.6 μm compared to 0.1 μm in the vibropolished sample. This difference is due to numerous new diffusion paths for oxygen created by new dislocations and grain boundaries in the electropolished specimen. In contrast to the vibropolished sample, cracks could form from the pores in the tribo-oxide, leading to delamination at the surface.
iii) A difference was observed in the plowing process: during the tribological testing of the electropolished specimen with many small sintering pores, material was smeared at the surface into the sintering pores, whereas in the vibropolished specimen with many sintering pores, sintered particles were pushed down into the subsurface sintering pores.

All these phenomena occurring in the electropolished specimen with many sintering pores were also observed in the vibropolished specimens with few sintering pores. Since they exhibited a similar trend in the coefficient of friction over the 1000 cycles, deformation, tribo-oxidation, cracks, and delamination can be associated with the presence of a high coefficient of friction.

The second part of this manuscript investigated whether, despite minimal subsurface deformation in vibropolished specimens with many sintering pores, an increase in cycles from 1000 to 5000 could advance tribo-oxidation to such an extent that the tribological behavior resembled that of vibropolished specimens with few sintering pores or the electropolished sample with many sintering pores. The following conclusion can be drawn:

iv) In the vibropolished specimens with many sintering pores, no changes were observed after 5000 cycles, except for an increase in tribo-oxidation depth from 0.3 to 0.5 μm. However, an increase in cycles resulted in cracks in the tribo-oxide and surface delamination in the vibropolished specimen with few, small sintering pores, indicating that these phenomena emerge as tribo-oxidation progresses. For specimens with many sintering pores, a considerable increase in cycles is probably necessary for this to happen.

The results of this study highlight the importance of surface treatment tailored to the manufacturing process of the workpiece and the impact of improper preparation method on the tribological behavior, not only within the first cycles but also for at least 5000 cycles. Since the findings are in all likelihood not specific to copper, it can be assumed that other materials could also benefit from such surface preparation routes.

These findings underscore critical design considerations for copper components intended for tribological applications. Specifically, achieving approximately 15 % porosity is essential to ensure long-term stability of low friction, in contrast to lower porosity levels. Furthermore, the feasibility of chemical–mechanical vibropolishing on sliding contact surfaces must be a fundamental aspect of the design process. Consequently, component geometries should be engineered to provide sufficient accessibility for effective surface treatment, avoiding complex features that impede polishing [70]. Such design strategies optimize the tribological behavior, thereby ensuring sustained low friction in applications including bearings, seals, and electrical contacts, and offer mass saving advantages.

CRediT authorship contribution statement

Roxane Lung: Writing – original draft, Visualization, Investigation, Data curation. **Karl Günter Schell:** Investigation, Methodology, Resources, Writing – review & editing. **Christian Greiner:** Writing – review & editing, Supervision, Resources, Project administration, Funding acquisition, Conceptualization.

Funding

This work was supported by the European Research Council under ERC Grant Agreement [No. 771237]; and by the German Research Foundation (DFG) [Project No. GR 4174/7].

Declaration of competing interest

The authors declare the following financial interests/personal relationships which may be considered as potential competing interests: Christian Greiner reports financial support was provided by German Research Foundation. Christian Greiner reports financial support was provided by European Research Council. If there are other authors, they declare that they have no known competing financial interests or personal relationships that could have appeared to influence the work reported in this paper.

Acknowledgments

The author would like to thank Dr. Daniel Schliephake for his support with the vibropolishing process and Malte Lauritz Flachmann for the scientific discussion.

Appendix A. Supplementary data

Supplementary data to this article can be found online at https://doi.org/10.1016/j.matdes.2025.114584.

Data availability

The raw data used for the analysis and evaluation of surfaces, subsurface microstructures and coefficients of friction, are published on KITopen DOI: 10.35097/128dk8w5sjjcv1en.

References

[1] G. Yang, B. Wang, K. Tawfiq, H. Wei, S. Zhou, G. Chen, Electropolishing of surfaces: theory and applications, Surf. Eng. 33 (2017) 149–166, https://doi.org/10.1080/02670844.2016.1198452.

[2] S. Zaki, N. Zhang, M.D. Gilchrist, Electropolishing and Shaping of Micro-Scale Metallic Features, Micromachines 13 (2022) 468, https://doi.org/10.3390/mi13030468.

[3] K.E. Herrera, Custom Cathode Optimization for Electropolishing Additively Manufactured 316L Stainless Steel, The University of New Mexico, Albuquerque, 2023. Master Thesis.

[4] T. Hryniewicz, Concept of microsmoothing in the electropolishing process, Surf. Coat. Technol. 64 (1994) 75–80, https://doi.org/10.1016/S0257-8972(09)90006-8.

[5] M. Sun, Development of Novel Surface Finishing Processes for Additively Manufactured Metal Parts, University of Waterloo, Waterloo, 2025. Ph.D. Thesis.

[6] Y. Zhou, M. Chai, F. Yan, Z. Li, Effects of electrochemical polishing on the surface properties of laser-cut Ni–Ti alloy cardiovascular stents, Int. J. Electrochem. Sci. 20 (2025), https://doi.org/10.1016/j.ijoes.2025.101101.

[7] X. Zhao, S. Wang, L. Liu, Q. Li, J. Yu, G. Wang, C. Liang, Z. Wang, H. Hao, X. Xu, L. Zhang, Advance Chemical Mechanical Polishing Technique for Gallium Nitride Substrate, Adv. Mater. Interfaces 12 (2025) 2301032, https://doi.org/10.1002/admi.202301032.

[8] X. Lei, Z. Zhang, H. Zhou, L. Chen, X. Deng, W. Liu, X. Zhuang, M. Wang, Y. Gu, Close atomic surface on aluminum alloy achieved by a near-neutral novel green chemical mechanical polishing method with high material removal rate, Nanoscale 17 (2025) 12684–12694, https://doi.org/10.1039/D5NR00132C.

[9] J.M. Steigerwald, S.P. Murarka, R.J. Gutmann, D.J. Duquette, Chemical processes in the chemical mechanical polishing of copper, Mater. Chem. Phys. 41 (1995) 217–228, https://doi.org/10.1016/0254-0584(95)01516-7.

[10] D. Zhao, X. Lu, Chemical mechanical polishing: Theory and experiment, Friction 1 (2013) 306–326, https://doi.org/10.1007/s40544-013-0035-x.

[11] U. Paik, J.-G. Park, Nanoparticle Engineering for Chemical-Mechanical Planarization: Fabrication of Next-Generation Nanodevices, Taylor & Francis, London, 2009.

[12] P.C. Brust, Surface improvement by vibratory cascade finishing process, Transactions of the North American Manufacturing Research Institute of SME (1997) 93–98.

[13] J. Domblesky, R. Evans, V. Cariapa, Material removal model for vibratory finishing, Int. J. Prod. Res. 42 (2004) 1029–1041, https://doi.org/10.1080/00207540310001619641.

[14] M.-Y. Tsai, W.-Z. Yang, Combined ultrasonic vibration and chemical mechanical polishing of copper substrates, Int. J. Mach. Tool Manuf. 53 (2012) 69–76, https://doi.org/10.1016/j.ijmachtools.2011.09.009.

[15] H. Chen, D. Guo, G. Xie, G. Pan, Mechanical model of nanoparticles for material removal in chemical mechanical polishing process, Friction 4 (2021) 153–164, https://doi.org/10.1007/s40544-016-0112-z.

[16] K. Ahluwalia, R. Mediratta, S.H. Yeo, A novel approach to vibratory finishing: double vibro-polishing, Mater. Manuf. Process. 32 (2017) 998–1003, https://doi.org/10.1080/10426914.2016.1232812.

[17] K. Holmberg, A. Erdemir, Influence of tribology on global energy consumption, costs and emissions, Friction 5 (2017), 263–284. https://doi.org /10.1007/s40544-017-0183-5.

[18] R. Lung, K. G. Schell, C. Greiner, Porosity Matters: Exploring its Impact on the Unlubricated Tribological Behavior of Copper, under consideration (2025). https://doi.org/10.35097/q9q7nbnb7ggazf4m.

[19] M. F. C. Ordoñez, D. L. Rodrigues, A. P. Tschiptschin, R. M. Souza, Effect of porosity on surface deformation and subsurface layer produced by scratch tests of sintered low-alloy steel, Tribology International 209 (2025), 110674. https://doi.org /10.1016/j.triboint.2025.110674.

[20] A. Sinha, Z. Farhat, Effect of Surface Porosity on Tribological Properties of Sintered Pure Al and Al 6061, Mater. Sci. Appl. 06 (2015) 549, https://doi.org/10.4236/msa.2015.66059.

[21] F. Martin, C. García, Y. Blanco, Influence of residual porosity on the dry and lubricated sliding wear of a powder metallurgy austenitic stainless steel, Wear 328–329 (2015) 1–7, https://doi.org/10.1016/j.wear.2015.01.025.

[22] R.A. Al-Samarai, K.R.A. Haftirman, Y. Al-Douri, The influence of roughness on the wear and friction coefficient under dry and lubricated sliding, Int. J. Sci. Eng. Res. 3 (4) (2012) 1–6.

[23] K.J. Kubiak, T.W. Liskiewicz, T.G. Mathia, Surface morphology in engineering applications: Influence of roughness on sliding and wear in dry fretting, Tribol. Int. 44 (2011) 1427–1432, https://doi.org/10.1016/j.triboint.2011.04.020.

[24] F. Svahn, Å. Kassman-Rudolphi, E. Wallén, The influence of surface roughness on friction and wear of machine element coatings, Wear 254 (2003) 1092–1098, https://doi.org/10.1016/S0043-1648(03)00341-7.

[25] G. Liang, S. Schmauder, M. Lyu, Y. Schneider, C. Zhang, Y. Han, An Investigation of the Influence of initial Roughness on the Friction and Wear Behavior of Ground Surfaces, Materials 11 (2018) 237, https://doi.org/10.3390/ma11020237.

[26] F.P. Bowden, A.J.W. Moore, D. Tabor, The Ploughing and Adhesion of Sliding Metals, J. Appl. Phys. 14 (1943) 80–91.

[27] C. Greiner, Z. Liu, L. Strassberger, P. Gumbsch, Sequence of Stages in the Microstructure Evolution in copper under Mild Reciprocating Tribological Loading, ACS Appl. Mater. Interfaces 8 (2016) 15809–15819, https://doi.org/10.1021/acsami.6b04035.

[28] D.A. Rigney, J.E. Hammerberg, Unlubricated Sliding Behavior of Metals, MRS Bull. 23 (1998) 32–36, https://doi.org/10.1557/S0883769400030608.

[29] D.A. Hughes, N. Hansen, Graded Nanostructures Produced by Sliding and Exhibiting Universal Behavior, Phys. Rev. Lett. 87 (2001) 135503, https://doi.org/10.1103/PhysRevLett.87.135503.

[30] N. Argibay, M. Chandross, S. Cheng, J.R. Michael, Linking microstructural evolution and macro-scale friction behavior in metals, J. Mater. Sci. 52 (2017) 2780–2799, https://doi.org/10.1007/s10853-016-0569-1.

[31] Z. Liu, C. Patzig, S. Selle, T. Höche, P. Gumbsch, C. Greiner, Stages in the tribologically-induced oxidation of high-purity copper, Scr. Mater. 153 (2018) 114–117, https://doi.org/10.1016/j.scriptamat.2018.05.008.

[32] Z. Liu, Microstructure evolution under tribological loading and its elementary mechanisms, Karlsruhe Institute of Technology, Karlsruhe, 2018. Ph.D. Thesis.

[33] S.-K. Lee, H.-C. Hsu, W.-H. Tuan, Oxidation Behavior of copper at a Temperature below 300 °C and the Methodology for Passivation, Mater. Res. 19 (2016) 51–56, https://doi.org/10.1590/1980-5373-MR-2015-0139.

[34] H.Z. Hassan, N.M. Saeed, Advancements and applications of lightweight structures: a comprehensive review, Discover Civil Engineering 1 (2024) 47, https://doi.org/10.1007/s44290-024-00049-z.

[35] Y.F. Takele, A.D. Woldeyohannes, Optimal material selection for high temperature tribological application: an integrated multi criteria decision study, Discover Materials 5 (2025) 33, https://doi.org/10.1007/s43939-025-00209-7.

[36] A. Candela, G. Sandrini, M. Gadola, D. Chindamo, P. Magri, Lightweighting in the automotive industry as a measure for energy efficiency: Review of the main materials and methods, Heliyon 10 (2024), https://doi.org/10.1016/j.heliyon.2024.e29728.

[37] Y. Liu, Y. Li, L. Miao, Impact of lightweight materials substitution on material stock and carbon emission of private vehicles in China, Environment, Development and Sustainability (2024) 1–24, https://doi.org/10.1007/s10668-024-04762-8.

[38] M.L. Rahaman, E. Bernal, M. Spiryagin, C. Cole, R. Buckley, Q. Wu, A review on frictional torque reduction approaches for energy efficient roller bearings, Adv. Mech. Eng. 17 (2025) 16878132251340233, https://doi.org/10.1177/16878132251340233.

[39] C. Vincent, J.F. Silvain, J.M. Heintz, N. Chandra, Effect of porosity on the thermal conductivity of copper processed by powder metallurgy, J. Phys. Chem. Solid 73 (2012) 499–504, https://doi.org/10.1016/j.jpcs.2011.11.033.

[40] G. Singh, S. Singh, J. Singh, P.M. Pandey, Parameters effect on electrical conductivity of copper fabricated by rapid manufacturing, Mater. Manuf. Process. 35 (2020) 1769–1780, https://doi.org/10.1080/10426914.2020.1784937.

[41] Q. Mao, Y. Liu, Y. Zhao, A review on copper alloys with high strength and high electrical conductivity, J. Alloy. Compd. 990 (2024) 174456, https://doi.org/10.1016/j.jallcom.2024.174456.

[42] G. Zhou, Y. Qiao, Study on Heat transfer of Copper Foam Microstructure in phase Change Materials, Sustainability 17 (2025) 1681, https://doi.org/10.3390/su17041681.

[43] W. F. Koch, R. S. Davis, V. E. Bower, Direct Determination of Air Density in a Balance Through Artifacts Characterized in an Evacuated Weighing Chamber., Journal of Research of the National Bureau of Standards 83 (1978), 407–413. https://doi.org/ 10.6028/jres.083.026.

[44] N.A. Lange Lange's Handbook of Chemistry J.A. Dean Inorganic Chemistry Ch. 3 15. ed, 1999 McGraw-Hill New York.

[45] G. T. Beilby, Aggregation and Flow of Solids: Being the Records of an Experimental Study of the Micro-structure and Physical Properties of Solids in Various States of Aggregation, 1900-1921, Macmillan and Company, 1921.

[46] T.P. Hoar, J.A.S. Mowat, Mechanism of Electropolishing, Nature 165 (1950) 64–65, https://doi.org/10.1038/165064a0.

[47] A. Buch, S. Goldschmidt, Influence of porosity on elastic moduli of sintered materials, Mater. Sci. Eng. 5 (1970) 111–118, https://doi.org/10.1016/0025-5416(70)90040-6.

[48] M. Fellah, N. Hezil, D. Bouras, A. Obrosov, A.S. Mohammed, A. Montagne, A. Abd-Elmonem, S.M. El Din, S. Weiß, Structural, mechanical and tribological performance of a nano structured biomaterial Co–Cr–Mo alloy synthesized via mechanical alloying, J. Mater. Res. Technol. 25 (2023) 2152–2165, https://doi.org/10.1016/j.jmrt.2023.06.031.

[49] A. Charvátová Campbell, V. Buršíková, J. Martinek, P. Klapetek, Modeling the influence of roughness on nanoindentation data using finite element analysis, International Journal of Mechanical Sciences 161–162 (2019) 105015, https://doi.org/10.1016/j.ijmecsci.2019.105015.

[50] I. Green, Poisson Ratio Effects and critical Values in Spherical and Cylindrical Hertzian Contacts, Appl. Mech. Eng. 10 (2005) 3.

[51] V.L. Popov, Verschleiß, in: V.L. Popov (Ed.), Kontaktmechanik Und Reibung: Ein Lehr- Und Anwendungsbuch Von Der Nanotribologie Bis Zur Numerischen Simulation, Springer, Berlin, Heidelberg, 2009, pp. 263–276.

[52] V.L. Popov, Rigorose Behandlung des Kontaktproblems – Hertzscher Kontakt, in: V. L. Popov (Ed.), Kontaktmechanik Und Reibung: Von Der Nanotribologie Bis Zur Erdbebendynamik, Springer, Berlin, Heidelberg, 2010, pp. 59–74.

[53] V. Popov, Das Coulombsche Reibungsgesetz, in: V.L. Popov (Ed.), Kontaktmechanik Und Reibung: Von Der Nanotribologie Bis Zur Erdbebendynamik, Springer, Berlin, Heidelberg, 2010, pp. 137–159.

[54] F.P. Bowden, D. Tabor, The Friction and Lubrication of Solids, Clarendon Press, Oxford, 2001.

[55] I. Platzman, R. Brener, H. Haick, R. Tannenbaum, Oxidation of Polycrystalline Copper Thin Films at Ambient Conditions, J. Phys. Chem. C 112 (2008) 1101–1108, https://doi.org/10.1021/jp076981k.

[56] J.J.D. León, D.M. Fryauf, R.D. Cormia, N.P. Kobayashi, Study of the formation of native oxide on copper at room temperature, Low-Dimensional Materials and Devices 2016 (9924) (2016) 63–69, https://doi.org/10.1117/12.2238745.

[57] J.S. Rau, S. Balachandran, R. Schneider, P. Gumbsch, B. Gault, C. Greiner, High diffusivity pathways govern massively enhanced oxidation during tribological sliding, Acta Mater. 221 (2021) 117353, https://doi.org/10.1016/j.actamat.2021.117353.

[58] D. Hull, D.J. Bacon, Strength of Crystalline Solids, in: D. Hull, D.J. Bacon (Eds.), Introduction to Dislocations, fifth ed., Butterworth-Heinemann, Oxford, 2011, pp. 205–249.
[59] H. Magnusson, K. Frisk, Self-diffusion and impurity diffusion of hydrogen, oxygen, sulphur and phosphorus in copper, accessed 2025-04-15, Technical Report SKB (2013), https://www.skb.se/publication/2477839/TR-13-24.pdf.
[60] J. Li, J.W. Mayer, E.G. Colgan, Oxidation and protection in copper and copper alloy thin films, J. Appl. Phys. 70 (1991) 2820–2827, https://doi.org/10.1063/1.349344.
[61] J.S. Lehmann, R. Schwaiger, M. Rinke, C. Greiner, How Tribo-Oxidation Alters the Tribological Properties of copper and its Oxides, Adv. Mater. Interfaces 8 (2021) 2001673, https://doi.org/10.1002/admi.202001673.
[62] N.P. Suh, The delamination theory of wear, Wear 25 (1973) 111–124, https://doi.org/10.1016/0043-1648(73)90125-7.
[63] A. Ponomarenko, D. Quéré, C. Clanet, A universal law for capillary rise in corners, J. Fluid Mech. 666 (2011) 146–154, https://doi.org/10.1017/S0022112010005276.
[64] Wm. H. Ross, R. M. Jones, C. B. Durgin, The Purification of Phosphoric Acid by Crystallization, Industrial & Engineering Chemistry 17 (1925), 1081–1083. https://doi.org/ 10.1021/ie50190a031.
[65] M.M.S.H. Tang, Purification of phosphoric acid by melt crystallization, Martin-Luther-Universität Halle-Wittenberg, Halle, 1988. Ph.D. Thesis.
[66] H.R. Corti, F.J. Nores-Pondal, C. Austen Angell, Heat capacity and glass transition in P 2 O 5 –H 2 O solutions: support for Mishima's conjecture on solvent water at low temperature, PCCP 13 (2011) 19741–19748, https://doi.org/10.1039/c1cp22185j.
[67] Z. Bakher, M. Kaddami, Liquid–Liquid–Solid Equilibria in the Ternary System Water–Phosphoric Acid–Cyclohexane at 25 and 35 °C: Stability Domain of Hemihydrate and Anhydrous Phosphoric Acid, J. Chem. Eng. Data 64 (2019) 161–168, https://doi.org/10.1021/acs.jced.8b00666.
[68] B.M.H. Gorenflo, Plastic deformation of copper under variable tribological load, Karlsruhe Institute of Technology, Karlsruhe, 2021. Master Thesis.
[69] M.L. Flachmann, Copper tribology under a variety of loading conditions and oxidation regimes. The Case for Efficient Analysis via FAIR Data, Master Thesis, Karlsruhe Institute of Technology, Karlsruhe, 2023.
[70] X. Chen, Z. Zhang, F. Zhao, H. Luo, J. Wang, F. Meng, H. Zhou, X. Zhuang, G. Li, Review on chemical mechanical polishing for atomic surfaces using advanced rare earth abrasives, J. Phys. D Appl. Phys. 58 (2024) 023004, https://doi.org/10.1088/1361-6463/ad8453.